Behavior of Saline Ice under Cyclic Flexural Loading

Andrii Murdza[1], Erland M. Schulson[1], Carl E. Renshaw[1,2]

[1]Thayer School of Engineering, Dartmouth College, Hanover, NH, USA, 03755
[2]Department of Earth Sciences, Dartmouth College, Hanover, NH, USA, 03755

Correspondence to: Andrii Murdza (Andrii.Murdza@dartmouth.edu)

Abstract. New systematic experiments reveal that the flexural strength of saline S2 columnar-grained ice loaded normal to the columns can be increased upon cyclic loading by about a factor of 1.5. The experiments were conducted using reversed cyclic loading over ranges of frequencies from 0.1 to 0.6 Hz and at a temperature of -10 ℃ on saline ice of two salinities: 3.0±0.9 and 5.9±0.6 ‰. Acoustic emission hit rate during cycling increases with an increase of stress amplitude of cycling. Flexural strength of saline ice of 3.0±0.9 ‰ salinity appears to increase linearly with increasing stress amplitude, similar to the behavior of laboratory-grown freshwater ice (Murdza et al., 2020b) and to the behavior of lake ice (Murdza et al., 2021). The flexural strength of saline ice of 5.9±0.6 ‰ depends on the vertical location of the sample within the thickness of an ice puck; i.e., the strength of the upper layers, which have a lower brine content, was found to be as high as three times that of lower layers. The fatigue life of saline ice is erratic. Cyclic strengthening is attributed to the development of an internal back stress that opposes the applied stress and originates possibly from dislocation pileups.

1. Introduction

Fatigue of materials is a subject of practical importance in engineering and has been widely studied (Bathias and Pineau, 2013; Broek, 1986; Schijve, 2009; Suresh, 1998). Fatigue refers to changes in material properties resulting from cyclic loading. Fatigue strength of crystalline materials is typically controlled by microcrack initiation and subsequent growth that leads to failure.

It is not surprising that fatigue appears to play an important role in sea ice mechanics. For example, the Arctic and Antarctic floating ice covers and ice shelves are subjected to cyclic loading from ocean swells that can penetrate deeply into an ice pack and potentially result in the breakup of the ice cover (Squire, 2007). Such events, where under the action of surface waves a floating ice cover exhibited sudden breakup into smaller pieces, have been repeatedly witnessed and described (Shackleton, 1982; Liu and others, 1988; Prinsenberg and Peterson, 2011; Asplin and others, 2012; Collins and others, 2015; Kohout and others, 2016; Hwang and others, 2017). Ice cover breakup leads to a decline in albedo (Pistone and others, 2014; Zhang and others, 2019) and to the acceleration of melting. Also, smaller ice floes attenuate ocean waves less effectively than does the parent solid ice cover, thereby endangering coastal zones to erosion. Given the retreat of the sea ice cover and the attendant increase in oceanic fetch, larger waves are expected to develop; correspondingly, the remaining ice cover is expected to be subjected to episodes of greater cyclic loading. The potential for fatigue failure is thus increasing.

34

35   Cyclic loading may also play an important role in other scenarios. For instance, during ice-structure
36   interactions (Jordaan, 2001; Hendrikse and Metrikine, 2016; O'Rourke and others, 2016; Jordaan and others, 2008)
37   the structure itself, such as a light-house, may be weakened or damaged to a degree that depends on the strength of
38   the ice. Other examples are runways and roads that are built by freezing water on cold oceans, rivers and lakes and
39   subsequently subject to cyclic loading. Therefore, it is important to understand the behavior of ice under cyclic
40   loading.

41

42   Currently, the effects of cyclic loading on the physical and mechanical properties of sea ice and on the
43   susceptibility of the material to fatigue are poorly constrained. Tabata and Nohguchi (1980) conducted experiments
44   on sea ice sampled from Lake Saroma, Hokkaido, Japan and from Barrow, Alaska. They loaded the ice cyclically
45   under uniaxial compression between two specified stress levels under a variety of combinations of strain rate (from
46   10^{-5} s^{-1} to 10^{-2} s^{-1}), temperature (from -2 °C to -24 °C) and orientation (horizontal and vertical). They found that
47   with a decrease of average stress and with a decrease of amplitude, the time to failure increases; and by lowering the
48   temperature, the time to failure and the number of cycles also increases.

49

50   Other evidence of the weakening of sea ice under wave-driven in situ cyclic loading is discussed by
51   Haskell and others (1996), Bond and Langhorne (1997), Langhorne and others (1998), (1999), (2001). In these
52   works the authors obtained an S-N fatigue curve (S, upper peak stress of cycling; N, number of cycles imposed to
53   failure), typical of curves obtained from engineering materials, i.e. for lower stress amplitude more cycles are
54   needed for failure. The authors stated that the endurance limit, that is the stress amplitude below which the sea ice
55   can withstand an unlimited number of cycles, is approximately one-half the failure stress of non-cycled ice.

56

57   The constitutive behavior of saline ice under cyclic loading was also investigated previously (Cole, 1995,
58   1998; Cole et al., 1998, 2002; Cole and Dempsey, 2004; Cole and Durell, 1995; Dempsey et al., 2003; Wei et al.,
59   2020); specifically, inelastic deformation of sea ice was explored and interpreted in terms of a dislocation-based
60   mechanism. In these works the authors investigated the effect of temperature (from -5 to -50 °C), microstructure
61   (total porosity varied from 14 to 104 ppt), cyclic stress amplitude (from 0.04 to 0.8 MPa), loading frequency (from
62   10^{-3} to 1 Hz), and dry isothermal vs floating specimens on the response of the ice. However, the strength of ice after
63   it had been cycled was not measured.

64

65   Nothing more (to our knowledge) has been reported on the fatigue of sea ice. The topic is absent from a
66   critical review by Squire (2007) and from two recent books on ice (Schulson and Duval, 2009; Weeks, 2010).

67

68   The behavior summarised above indicating the weakening of ice under cyclic loading, obtained from
69   experiments conducted on saline and sea ice, might possibly account for the sudden breakup of natural ice covers.
70   However, this behavior appears in conflict with the behavior of freshwater ice under cyclic loading (Cole, 1990;

Gupta et al., 1998; Iliescu et al., 2017; Iliescu and Schulson, 2002; Murdza et al., 2019, 2020b, 2020a). In those experiments, it was discovered that the ice flexural strength increases upon repetitive loading, followed by the recovery of the cyclic-induced increment in strength to the original non-cycled strength upon post-cycling annealing. This difference in the behavior of the two kinds of ice could perhaps be attributed to the presence of defects in sea/saline ice, such as brine pockets , brine channels and non-penetrating microcracks. Such defects serve as stress concentrators, thereby lessening the need to nucleate cracks to the degree that fatigue life may be governed primarily by crack propagation. The strengthening of ice is of more than scientific interest, reflected, perhaps in an interesting comment of an arctic engineer who reported that builders of ice roads never trust the ice until it had been "worked in" (Masterson, 2018).

Therefore, given that limited information about the behavior of sea/saline ice under cyclic loading and given the discrepancy in behavior of fresh and sea/saline ice, we conducted a study under controlled conditions in the laboratory on the flexural behavior of saline ice. In this paper, we describe the experiments in which beams of S2 columnar-grained saline ice of two salinities (3.0±0.9 and 5.9±0.6 ‰) were subjected at -10 ºC to four-point, reverse cycling at ~0.1-0.6 Hz and then, after several hundred or more cycles, were bent to failure, provided the beams did not break during cycling. We chose the rate of cycling to simulate the vibration frequency of a natural sea ice cover (Collins et al., 2015).

2. Experimental procedure

2.1 Ice growth and characterization

We studied saline ice of two melt-water salinities: 3.0±0.9 and 5.9±0.6 ppt, where ± sign indicates standard deviation. We produced the ice in the laboratory in an 800 L circular polycarbonate tank in the manner described previously (Golding et al., 2014). Briefly, solutions containing 17.5 ± 0.2 ppt and 35 ± 0.2 ppt (parts per thousand, or ‰) of the commercial product "Instant Ocean" salt mixture were prepared and then frozen unidirectionally downward over a period of about 7 days by using a top-placed cold plate maintained at a temperature $T = -20\pm0.1$ °C. Before bringing the cold plate into contact with the salt-water solution, the top surface of the solution was seeded with freshwater ice fragments of ~ 0.3 - 1 mm in diameter. This procedure produced pucks ~1 m in diameter and ~0.3 m thick. For practical considerations, the bottom, skeletal layer of ice of about 7-10 cm was discarded as it was slushy and weak; we also believe that the skeletal layer does not play a significant role in supporting load. The top layer of ice of a few centimeters was also discarded because it was seeded and its grain size was considerably smaller and its microstructure thus different from the rest of the ice puck. Melt-water salinity was measured using a calibrated YSI Pro30 conductivity and salinity probe.

Figure 1 shows the microstructure of the ice. Table 1 lists its density and the average grain size of the test specimens described below. Figure 2 shows stereographic projections of the orientation of the crystallographic c-axes. The ice is characterized by columnar-shaped grains whose growth texture is marked by c-axes confined within

106 about 15° of the horizontal plane of the parent ice puck and randomly oriented within that plane. In other words, the
107 ice is termed S2, after Michel and Ramseier (1971), and is similar to natural first-year sea ice (for comparison, see
108 Figure 3.7 of Schulson and Duval (2009)). The grain size noted above is the averge diameter of the columnar-shaped
109 grains, ranging from about 2 to 7 mm in Figure 1.

2.2. Growth features

111   The ice contained both sub-mm sized brine pockets and supra-mm sized drainage channels, reminiscent of
112 natural sea ice. Figures 3 and 4 show examples. The ice of lower salinity (3.0±0.9 ppt) had fewer defects of both
113 kinds. Some of the ice of higher salinity (5.9±0.6 ppt) possessed channels whose size was almost as large as the
114 grain diameter. The defects scattered light to the degree that in bulk form the ice had an overall opaque appearance.
115 When observed in thin section (~1mm) the ice exhibited to the naked eye distinct linear whitish features which we
116 took to be sets of interconnected brine pockets that could possibly be filled with very fine-grained ice. The ice of
117 higher salinity possessed more of these features, especially near the bottom of the parent puck (which was the last
118 part to solidify). Our sense is that these features served as stress concentrators, particularly ones that traversed the
119 width of the test specimen (described below), thereby weakening the ice. Indeed, as will become apparent, samples
120 obtained from near the bottom of a puck of higher salinity (5.9±0.6 ppt) had relatively low flexural strength.
121
122   Because the ice of both salinities exhibited a different appearance from the top and bottom of the parent
123 puck, in preparing test specimens for flexing we distinguished them by their position (depth from top surface) within
124 the ice puck from which they were prepared, Table 2.

2.3. Sample preparation and test setup

126   Once the ice had been grown, it was cut into blocks of dimensions ~ 10 x 30 x 20 cm^3, where the longest
127 and the shortest dimensions are in the horizontal plane of the original ice puck, perpendicular to the direction of
128 growth. The blocks were stored in a cooler (at -10±0.5 °C) on their side (such that columnar-shaped grains were
129 oriented horizontally) to reduce brine drainage for periods of time of about 1-10 weeks.
130
131   Specimens for flexing were manufactured from the ice blocks in the form of thin beams of dimensions
132 h ~16 mm in thickness (parallel to the long axis of the grains), b ~ 85 mm in width, and l ~300 mm in length. The
133 test specimens were allowed to equilibrate to the test temperature of -10 ± 0.5 °C for at least 24 hours before testing.
134
135   A detailed description of the specimens' preparation and loading can be found elsewhere (Iliescu et al.,
136 2017; Murdza et al., 2018, 2019, 2020b). To summarize: The ice beams were flexed up and down under 4-point
137 loading under constant displacement rate using a servo-hydraulic loading system (MTS model 810.14) to which we
138 attached a custom-built 4-point loading frame, Figure 5. The hydraulic actuator was driven up and down under
139 displacement control with the load limited in both directions. A load cell, calibrated for both tension and

140   compression, and a linear variable differential transformer (LVDT) gauge were used for measurements of load and
141   displacement of the upper surface of the ice beam during cycling.

142

143   Acoustic emissions were recorded during cycling using a PCI-2 18-bit A/D system; its frequency response
144   was 3 kHz–3 MHz and its minimum acoustic emission (AE) amplitude detection threshold was set to 45 dB. We
145   used a micro 30STC sensor (9.5 mm diameter, 11 mm thickness) which was attached to the top surface of an ice
146   beam with a rubber band. Vacuum grease was used as the coupling agent between the sensor and the ice surface.

147

148   The experiments were performed in a cold room at a temperature of -10°C and at an outer-fiber center-
149   point displacement rate of 0.1 mm s^{-1} (or outer-fiber strain rate of about 1.4 x 10^{-4} s^{-1}). This displacement rate
150   resulted in an outer-fiber stress rate in the range from ∼ 0.3 to 0.5 MPa s^{-1}, outer-fiber stress amplitude in the range
151   from 0.35 to 1.2 MPa, outer-fiber strain amplitude in the range from ∼ 1 to 5 x 10^{-4} and frequencies in the range
152   from 0.1 to 0.6 Hz (i.e. periods from ∼10 to 1.5 sec). The period, as already noted, is similar to the period of ocean
153   swells (Collins et al., 2015). The major outer-fiber stress σ_f was calculated from the relationship (the loading span is
154   ½ of the support span):

155

$$\sigma_f = \frac{3PL}{4bh^2} \qquad (1)$$

156
157
158   where P is the applied load and L is the distance between the outer-pair of loading cylinders (shown in Figure 5b)
159   and is set by the geometry of the apparatus to be $L = 254$ mm.

160

161   We used two different loading procedures, as we did earlier in our study of S2 freshwater ice. Type I
162   loading was a completely reversed stress cycle with constant stress amplitude and mean stress of zero. Type II was
163   similar to Type I but incorporated an increasing multi-level (or step-level) stress amplitude. This second type of
164   loading essentially consisted of several Type I steps of increasing stress amplitudes. In the present study for stress
165   amplitudes below 0.7 MPa we used Type I loading. To cycle ice samples at stress amplitudes above 0.7 MPa, we
166   first pre-conditioned specimens through step-loading Type II procedure at progressively higher stress amplitude
167   levels, i.e. we cycled specimens for ∼300 times at each of the following stress amplitudes: 0.7, 0.75, 0.8, 0.85 MPa
168   and so on either until failure occurred or until a specific value of stress amplitude set by the operator (see Iliescu et
169   al. (2017) and Murdza et al. (2018) for details). To change stress amplitude the loading was stopped for ∼15 sec to
170   change settings. After pre-conditioning, the specimens were cyclically loaded according Type I loading at least 300
171   times and generally for ∼2000 times, since no change in strength was observed beyond a few hundred cycles (see
172   below).

173

174   Figure 6 shows measurements of load and of displacement versus time at the beginning and near the end of
175   cycling before specimen failure of a lower-salinity specimen (3.0±0.9 ppt). The measurements detected   no

176 softening. According to Bažant et al. (1984) softening is a decline of stress at increasing strain or, in our case, an
177 increase of strain during cycling at constant stress amplitude during the tests). The absence of detectable softening
178 during cycling of the saline ice is reminiscent of the absence of softening during the cycling of freshwater ice
179 (Iliescu et al., 2017; Murdza et al., 2020b).

180 **3. Results and Observations**

181 **3.1. Flexural strength of non-cycled ice**

182   The flexural strength of non-cycled saline ice of both salinities was measured at -10 ºC and at a nominal
183 outer-fiber center-point displacement of 0.1 mm s^{-1}. The results are listed in Table 2. Failure more often occurred at
184 random locations between the two inner loading cylinders and less often either below or slightly outside the loading
185 cylinders. The reason for the latter location was the presence prior to testing of a significant concentration of whitish
186 features at loading cylinders which served as stress concentrators and along which the failure ultimately occurred
187 (similar to Figure 4). The average and standard deviation of the measured flexural strength of saline ice of lower
188 salinity (3.0±0.9 ppt) are 0.96±0.13 MPa. The strength of the lower salinity ice did not correlate systematically with
189 the depth of the parent puck from which ice beams were prepared. The measured strength compares favorably with
190 the value of 0.85±0.20 MPa reported by Timco and O'Brien (1994) for sea ice of similar salinity, as can be seen in
191 Figure 7. Brine volume fraction v_b was calculated according to Frankenstein and Garner (1967):
192

$$v_b = 0.001 * S\left(\frac{49.185}{|T|} + 0.532\right), \tag{2}$$

193
194 where T is temperature in degrees Celsius between -0.5 °C and -22.9 °C and S is melt-water salinity (in ppt) of the
195 ice.
196
197   The average and standard deviation of the measured flexural strength of saline ice of higher salinity
198 (5.9±0.6 ppt) are 0.98±0.36 MPa. The measured values (Figure 7) deviate slightly towards higher values compared
199 to the data of Timco and O'Brien (1994), although scatter is significantly greater than is the scatter in the strength of
200 the ice of lower salinity (3.0±0.9 ppt). This may be explained by the greater degree of interconnectivity of brine
201 pockets at the bottom of an ice puck (discussed above and shown in Figures 3 and 4). Indeed, the flexural strength of
202 the higher-salinity specimens appears to depend on the depth of ice from which beams were prepared, Table 2. This
203 result shows how much the strength of ice is sensitive to flaws and defects. Given that larger bodies usually contain
204 larger defects, the flexural strength of sea ice on the medium and large scale, in the field (Karulina et al., 2013,
205 2019; Murdza et al., 2016) for instance, is expected to be lower than on the smaller scale of the present experiments.
206
207   We also compare our measurements of flexural strength with the tensile strength of sea ice. For this
208 purpose, and as we did in our previous work on freshwater ice (Iliescu et al., 2017; Murdza et al., 2020b), flexural

strength is divided by 1.7 (Ashby and Jones, 2012). This factor reflects the fact that the volume of the material which is subjected to the highest stress in bending is smaller than in uniaxial tension; thus, the largest defect which governs the failure may not be near the surface of a bent specimen. Upon dividing the flexural strength of the non-cycled saline ice of lower salinity by 1.7, we found the average across-column tensile strength from our experiments to be 0.96±0.13 MPa/1.7 = 0.56±0.08 MPa. This value compares favorably with the values 0.56±0.06 MPa and 0.63±0.12 MPa reported by Richter-Menge and Jones (1993) for the tensile strength of columnar-grained first-year sea ice of 4.1±0.3 ppt salinity loaded uniaxially across the columns at a temperature of -10 °C and strain rates of 10^{-5} and 10^{-3} s^{-1}. Recall that in the present experiments the outer-fiber strain rate was about 1.4 x 10^{-4} s^{-1} which is within the range reported by Richter-Menge and Jones (1993). This agreement between direct and indirect measurements of tensile strength lends confidence that our lab-grown saline ice is a reasonably faithful analogue of natural sea ice.

3.2. Flexural strength versus number of reversed cycles under constant low stress amplitude

To determine whether there is a relationship between flexural strength and number of cycles imposed under a constant low stress amplitude, we performed via Type-I loading a series of experiments on saline ice of lower salinity (3.0±0.9 ppt) at -10 °C at an outer-fiber center-point displacement rate of 0.1 mm s^{-1} at a low stress amplitude of 0.35 MPa; i.e., at an amplitude less than one-half the flexural strength of non-cycled ice. Figure 8 shows the results. The number of cycles varied from about 100 to 14000. The average strength and standard deviation of all data from Figure 8 are 0.96±0.23 MPa. As noted above the strength and standard deviation of non-cycled ice are 0.96±0.13 MPa. In other words, no strengthening was detected upon cycling up to 14000 times at a stress amplitude of 0.35 MPa. For freshwater ice (Murdza et al., 2020b), we found that once the number of cycles at a given low stress amplitude exceeded 300, the number of cycles had no significant effect on the flexural strength, implying that a kind of saturation of strength developed. Given that result and the new resuts for saline ice, we followed the practice in the present study of cycling more than 300 times, often as many as 2000 times, before bending the ice to failure.

3.3. Flexural strength versus stress amplitude

The flexural strength increases with stress amplitude. Figure 9 shows measurements obtained from saline ice of both salinities cycled at -10 ° C at an outer-fiber displacement rate of 0.1 mm s^{-1}. For comparison, data from laboratory grown freshwater ice (Murdza et al., 2020b) of S2 character and from lake ice of the same character (Murdza et al., 2020a, 2021) are also shown. The relationship between the flexural strength, σ_{fc} and cycled stress amplitude, σ_a, for saline ice appears to be a linear one and, within experimental scatter, to have essentially the same sensitivity to stress amplitude as freshwater ice; namely:

$$\sigma_{fc} = \sigma_{f0} + k\sigma_a \ , \tag{3}$$

241 where $k = 0.68$ is a constant. For freshwater ice the non-cycled flexural strength is $\sigma_{f0} = 1.75$ MPa compared with

242 $\sigma_{f0} = 0.96$ MPa for the saline ice. There is, perhaps, in Figure 9 a hint that for saline ice there is a threshold of

243 about 0.4 MPa that must be exceeded to detect strengthening. Interestingly, this apparent threshold is similar in

244 magnitude to the stress that marks the onset of significant AE activity under cyclic loading of sea ice cores (Cole

245 and Dempsey, 2006). Although saline ice is weaker than freshwater ice, it appears that upon cycling its strength

246 increases at the same rate as freshwater ice.

247

248 Although the rate of strengthening with stress amplitude appears to be the same for sline ice and freshwater

249 ice, the maximum increase in strength in the case of saline ice of lower salinity (3.0±0.9 ppt) is significantly lower.

250 We were able to strengthen saline ice by about 50% of the non-cycled strength compared with about 100% for

251 freshwater ice (Murdza et al., 2020b). Another point is that we almost were not able to cycle specimens at stress

252 amplitudes greater than the flexural strength of non-cycled material, whereas in the case of freshwater ice we were

253 able to cycle at stress amplitudes significantly greater than flexural strength of non-cycled ice. Indeed, the maximum

254 cycled stress amplitude we were able to reach in the case of saline ice of lower salinity (3.0±0.9 ppt) during all tests

255 was 1.1 MPa, which is not statistically different from the non-cycled flexural strength of 0.96±0.13 MPa.

256

257 For saline ice of lower salinity (3.0±0.9 ppt), there is no evidence that the flexural strength of both non-

258 cycled and cycled ice is significantly affected by the depth of ice from which ice beams were harvested. For saline

259 ice of higher salinity (5.9±0.6 ppt), however, the flexural strength of both non-cycled and cycled ice appears to

260 depend on the depth of ice from which beams were prepared, Figure 10. Indeed, the flexural strength of specimens

261 from the bottom and from the top of an ice puck of higher salinity (5.9±0.6 ppt) differs by ~3 times (~0.4 MPa vs

262 ~1.4 MPa).

263 **3.4. Fatigue behavior**

264 Although the specimens from which the data in Figure 9 were obtained did not fail during cycling, other

265 specimens cycled under similar consitions did fail while being cycled. Results from such tests (on of saline ice of

266 lower salinity (3.0±0.9 ppt) at -10ºC and 0.1 mm s^{-1} outer-fiber displacement rate) allowed us to construct S-N

267 fatigue curve , shown in Figure 11. The number of cycles here is the number of cycles to failure during cycling at

268 the last stress amplitude level and not the total number of cycles. At most the S-N curve showd only a weak

269 systematic dependence of the number of cycles to failure on stress amplitude. Indeed, for the same stress amplitude

270 of ~ 0.9 MPa, fatigue failure occurred after as few as <10 cycles and after as many as a few thousand cycles.

271 Statistical analyses to test the hypothesis that the slope in Figure 11 is zero resulted in a p-value equal ~0.06.

272 Therefore, there is only a marginally significant effect of number of cycles on the stress at which failure occurred.

273 We attribute this variability in fatigue life to the variability in microstructure from specimen to specimen.

274

That said, a note of caution is appropriate. The data in Figure 11 should not be viewed as fatigue data in the usual sense; i.e., in the way such data are viewed when obtained from other materials (e.g., metals and alloys) that exhibit classical fatigue behavior. In those cases, before cycling, all specimens are assumed to have the same thermal-mechanical history. That was not the case here for the saline ice, as most of the samples were pre-conditioned according to Type II procedure before they were cycled at the last stress level where they failed while cycling. In other words, in order to get fatigue failure, we were increasing stress amplitude by small increments of ~0.05 MPa and allowed a sufficient number of cycles at each stress level (~500-1000) before we reached a fatigue failure.

The question to address here is why we did not obtain a classical S-N curve? We suggest that the classical mechanism of fatigue, i.e. accumulation of damage, is not in play in our tests and some other process is controlling fatigue life.

3.5 Microstructural observations of samples after fatigue failure

In an attempt to reveal deformation damage in the form of microscracks, we examined using thin-section optical microscopy (up to 50x magnification) the microstructure of specimens of the lower salinity ice (3.0±0.9 ppt) after they had failed during cycling; i.e., failed in fatigue. Three thin sections were prepared from four specimens in order to ensure a greater probability of observing microcracks growing from brine pockets or brine channels, should they be present. The plane of the thin section was parallel to the long axis of the columnar grains and parallel to the direction of the greater normal stress. This plane was taken as the best plane to observe possible cracks. Thin sections were observed using non-polarized light. We found no evidence of microcracks starting from brine pockets or from other defects. In fact, we found no microcracks at all. It appears, therefore, that slow crack growth is not a significant contribution to the fatigue life of the beams of the laboratory-grown saline ice that we studied.

3.6. Acoustic emissions

Acoustic emissions (AE) during repetitive loading of ice have been previously recorded and analyzed in laboratory and in situ (Langhorne and Haskell, 1996), (Cole and Dempsey, 2006, 2004; Lishman et al., 2020; Murdza et al., 2020b). Langhorne and Haskell (1996) suggested that the emissions originate either from dislocation breakaway or from microcracking associated with dislocation motion.

In contrast to freshwater ice, where no sound was detected until failure (Murdza et al., 2020b), continuous emission was detected while cycling at constant stress amplitude. Figure 12 shows the cummulative acoustic emissions, or "hits", as a function of time for ice that was cycled reversely at a constant stress amplitude of 0.5 MPa. As can be seen, the hit rate (or hits per unit time), which is the slope of the curve in Figure 12, is about the same for the duration of the experiment.

309   Interestingly, the hit rate depends on stress amplitude during cycling. Figure 13 shows this behavior . The

310   greater is the stress amplitude, the greater is the hit rate. However, during cycling below about 0.2 MPa no hits were

311   detected.

312

313   Figure 13 also indicates that the hit rate is independent of the sequence of different stress amplitudes.The

314   numbers in Figure 13 show the order of cycling at different stress amplitudes; i.e., firstly we cycled ice at higher

315   stress amplitudes (0.5-0.8 MPa), then at lower stress amplitudes (0.2-0.4 MPa). The results showed an increase in

316   the hit rate as stress amplitude increases, regardless of the sequence of cycling.

317   **4. Discussion**

318   The results obtained from the experiments described in this paper show that the flexural strength of saline

319   ice can be increased upon reversed cyclic loading. Therefore, the same set of questions as for the freshwater ice

320   should be addressed here, i.e.: What governs the flexural strength of saline ice? Does crack propagation or crack

321   nucleation control the tensile strength? First of all, to understand the behavior of saline ice, it is important to

322   recognize that flexural strength in the present experiments is governed by the tensile strength, although greater by a

323   factor of about 1.7 (Ashby and Jones, 2012). Secondly, the apparent absence of remnant microcracks within the two

324   parts of broken samples (Section 3.5) indicates that crack nucleation controls the flexural strength, just as it appears

325   to do for freshwater ice. Indeed, this seems reasonable given the fact that freshwater ice comprises of ~95% by

326   volume of the saline ice we studied. Within the freshwater component, there is almost no solubility of salts (Weeks

327   and Ackley, 1986). The remainder of the saline ice is a mixture of air and brine. As was shown earlier, the

328   microstructure of saline ice that we grew is closely similar to the microstructure of sea ice. Pores lower the saline ice

329   strength (Sammis and Ashby, 1986). However, the behavior of S2 saline ice under cyclic loading is essentially the

330   same as the behavior of S2 freshwater ice (Murdza et al., 2020b), i.e. its strength increases at the same rate as

331   freshwater ice upon cycling under a given amplitude of the outer fiber stress. Hence, it is reasonable to assume that

332   the strengthening mechanism for the saline ice is similar to that for the freshwater ice. In our earlier work (Murdza

333   et al., 2020b) we proposed that strengthening might be due to the development of an internal back stress that

334   originates from either dislocation pileups or grain boundary sliding. However, one reviewer suggested the

335   possibility of a different strengthening mechanism. Due to the inherent weakness of the saline ice microstructure, the

336   microstructural stress relief may occur through localized damage via microcracking mentioned above. More

337   research, however, is needed to examine this hypothesis.

338

339   The maximum degree of strengthening in the case of saline ice is significantly lower than that for the

340   freshwater ice, although the slopes of the two data sets (rate of strength increase with increasing cyclic amplitude) in

341   Figure 9 are nearly equivalent. That difference may be explained by the structure of saline ice which limits

342   maximum possible strengthening. Given the significantly greater number of stress concentrators in saline ice, such

343   as brine pockets and channels, the propensity for failure during cycling is greater in saline ice (Sammis and Ashby,

344   1986), thereby limiting the development of the back stress. Indeed, in the present study failure of specimens during

345   cycling occurred more frequently than in the study on freshwater ice (Murdza et al., 2020b).

346

347   Flexural experiments conducted on saline ice of higher salinity (5.9±0.6 ppt) showed the importance of

348   brine features. Samples that were manufactured from the bottom of the ice puck were characterized by more

349   frequent whitish interconnected features (taken to be interconnected brine pockets) that often were the path for easy

350   crack propagation. Often samples were so weak that they failed before testing simply by handling. Interestingly,

351   there were no interconnected features in samples prepared from the top of an ice puck, which resulted in a difference

352   of more than a factor of three in strength between samples from top and bottom. Samples produced from saline ice

353   of lower salinity (3.0±0.9 ppt) also had whitish features; however, these features were spread more uniformly (on a

354   macroscopic scale) across the sample, resulting in little difference in strength between the bottom and top samples.

355

356   It is worth noting again that a significantly greater fraction of saline ice samples failed in fatigue while pre-

357   conditioning compared with freshwater ice. This may be explained by the fact that freshwater ice was essentially

358   free from pores, brine pockets and other defects. Based on this observation, it appears that crack growth is not a

359   significant contribution to the fatigue life of saline ice under the conditions of our experiments.

360

361   On the origin of the acoustic emissions, there are at least four possible sources of the noise detected. One is

362   from microcracking. We imagine that microcracks form in regions of mechanical weakness which results in

363   accumulation of damage that we detected via the AE method. Specifically, the brine drainage whitish features

364   discussed above in the test specimens constitute regions of high porosity and thus provide favorable sites for the

365   concentration of such damage. Failure may occur when one of these sites can no longer support the applied stress

366   and a microcrack emerges from the damage zone and propagates. It is possible that newly formed microcracks are

367   stable until a critical length is reached (Cannon et al., 1990; Schulson et al., 1991), at which point the crack growth

368   ensues. The reason that microcracks were not observed under the optical microscope may be because they filled up

369   with liquid brine upon formation which results in a loss of contrast. A second possible explanation for the acoustic

370   emissions is the motion and friction of very fine particles of ice which may have been entrapped inside brine

371   drainage features, as mentioned above. A third possibility is microcracking along grain boundaries due to grain

372   boundary sliding (Elvin and Shyam Sunder, 1996; Goldsby and Kohlstedt, 1997; Mulmule and Dempsey, 1997;

373   Schulson et al., 1997; Weiss and Schulson, 2000). A fourth possible explanation consistent with the non-history

374   dependence of the hit rate (Figure 13) is a kind of water-hammer effect in which brine entrapped within pockets

375   impacts the wall, first in one direction and then another. None of these possibilities can be evaluated based upon the

376   limits of the present observations. We refrain, therefore, from further speculation on this point.

377

378   Returning to the observations noted in the Introduction, and to the results obtained from imposed, in situ

379   cyclic loading experiments on sea ice beams by (Bond and Langhorne, 1997; Haskell et al., 1996; Langhorne et al.,

380   1998, 1999), the question is: Why does ice fail in the field under wave action and under imposed cyclic loading, but

381 strengthen upon cycling in our experiments in the laboratory? Although we do not know the process through which
382 the ice sheet failed in the field, we expect that there are many micro and macro cracks in natural sea ice. Indeed,
383 thermally-induced tensile stresses can induce thermal cracking in floating ice sheets (Evans and Untersteiner, 1971).
384 Therefore, our sense is that the difference in ice behavior under cyclic loading in situ in the field (Bond and
385 Langhorne, 1997; Langhorne et al., 1998) and in the laboratory in the present study is due to other types of defects
386 other than brine channels and pockets that are generated in the field as a result of thermo-mechanical history of ice.

5. Conclusions

388 From new, systematic experiments on the flexural strength of sub-meter sized beams of S2 columnar-
389 grained saline ice stressed principally across the columns through reversed cyclic loading at a temperature of -10 °C
390 and frequencies in the range from 0.1 to 0.6 Hz, it is concluded that:

391 (i) The flexural strength of saline ice can be increased upon reversed cyclic loading by as much as 1.5 times.
392 (ii) The flexural strength of ice subsequent to cycling scales linearly with the amplitude of the outer-fiber
393 stress.
394 (iii) The fatigue life of saline ice is erratic and does not obey classical S-N behavior.
395 (iv) Crack growth is not a significant contribution to the fatigue life of saline ice.
396 (v) There is high variability in structure and strength through the thickness of a saline ice puck of higher
397 salinity (5.9±0.6 ppt).
398 (vi) Given the lack of definitive proof of the underlying failure mechanism in saline ice, the increase in flexural
399 strength of freshwater ice and saline ice attributable to pre-failure load cycling is roughly equivalent.
400 (vii) Acoustic emission hit rate during cycling at a constant stress amplitude is about constant.
401 (viii) Acoustic emission hit rate during cycling increases with an increase of stress amplitude of cycling.

Acknowledgements

403 We acknowledge helpful discussions/communications with Prof. Harold Frost, Dr. Robert Gagnon, and
404 Dr. Daniel Iliescu. We acknowledge thoughtful and helpful critical comments from two anonymous reviewers. This
405 work was supported by the US Department of the Interior-Bureau of Safety and Environmental Enforcement
406 (BSEE), contract no. E16PC00005 and by National Science Foundation (FAIN 1947-107).

408 **Author contributions:** AM, ES and CR designed the experiments and AM carried them out. AM prepared the
409 manuscript with contributions from all co-authors.

411 **Competing interests:** The authors declare that they have no conflict of interest.

412 **References**

413 Ashby, M. M. and Jones, D. R. H.: Engineering Materials 1: An Introduction to Properties, Applications and
414 Design., 2012.

415 Asplin, M. G., Galley, R., Barber, D. G. and Prinsenberg, S.: Fracture of summer perennial sea ice by ocean swell as
416 a result of Arctic storms, J. Geophys. Res. Ocean., 117(6), 1–12, doi:10.1029/2011JC007221, 2012.

417 Bathias, C. and Pineau, A.: Fatigue of Materials and Structures, edited by C. Bathias and A. Pineau, John Wiley &
418 Sons, Inc., Hoboken, NJ, USA., 2013.

419 Bažant, Z. P., Belytschko, T. B. and Chang, T.: Continuum Theory for Strain-Softening, J. Eng. Mech., 110(12),
420 1666–1692, doi:10.1061/(asce)0733-9399(1984)110:12(1666), 1984.

421 Bond, P. E. and Langhorne, P. J.: Fatigue behavior of cantilever beams of saline ice, J. Cold Reg. Eng., 11(2), 99–
422 112, doi:10.1061/(ASCE)0887-381X(1997)11:2(99), 1997.

423 Broek, D.: Elementary engineering fracture mechanics, 1st ed., Springer, Dordrecht., 1986.

424 Cannon, N. P., Schulson, E. M., Smith, T. R. and Frost, H. J.: Wing cracks and brittle compressive fracture, Acta
425 Metall. Mater., 38(10), 1955–1962, doi:10.1016/0956-7151(90)90307-3, 1990.

426 Cole, D. and Dempsey, J.: Laboratory observations of acoustic emissions from antarctic first-year sea ice cores
427 under cyclic loading, in 18th International POAC Conference, p. Vol 3, 1083-1092., 2006.

428 Cole, D. M.: Reversed direct-stress testing of ice: Initial experimental results and analysis, Cold Reg. Sci. Technol.,
429 18(3), 303–321, doi:10.1016/0165-232X(90)90027-T, 1990.

430 Cole, D. M.: A model for the anelastic straining of saline ice subjected to cyclic loading, Philos. Mag. A, 72(1),
431 231–248, doi:10.1080/01418619508239592, 1995.

432 Cole, D. M.: Modeling the cyclic loading response of sea ice, Int. J. Solids Struct., 35(31–32), 4067–4075,
433 doi:10.1016/S0020-7683(97)00301-6, 1998.

434 Cole, D. M. and Dempsey, J. P.: In situ Sea Ice Experiments in McMurdo Sound: Cyclic Loading, Fracture, and
435 Acoustic Emissions, J. Cold Reg. Eng., 18(4), 155–174, doi:10.1061/(ASCE)0887-381X(2004)18:4(155), 2004.

436 Cole, D. M. and Durell, G. D.: The cyclic loading of saline ice, Philos. Mag. A Phys. Condens. Matter, Struct.
437 Defects Mech. Prop., 72(1), 209–229, doi:10.1080/01418619508239591, 1995.

438 Cole, D. M., Johnson, R. A. and Durell, G. D.: Cyclic loading and creep response of aligned first-year sea ice, J.
439 Geophys. Res. Ocean., 103(C10), 21751–21758, doi:10.1029/98JC01265, 1998.

440 Cole, D. M., Dempsey, J., Kjestveit, G., Shapiro, S., Shapiro, L. and Morley, G.: The cyclic and fracture response of
441 sea ice in McMurdo Sound. Part I, in Proceedings of the 16th IAHR International Symposium on Ice, Dunedin, New
442 Zealand., 2002.

443 Collins, C. O., Rogers, W. E., Marchenko, A. and Babanin, A. V.: In situ measurements of an energetic wave event
444 in the Arctic marginal ice zone, Geophys. Res. Lett., 42(6), 1863–1870, doi:10.1002/2015GL063063, 2015.

445 Dempsey, J., Cole, D. M., Shapiro, S., Kjestveit, G., Shapiro, L. and Morley, G.: The cyclic and fracture response of
446 sea ice in McMurdo Sound. Part II, in Proceedings of the 17th International Conference onPort and Ocean
447 Engineeringunder Arctic Conditions, Trondheim, Norway. [online] Available from:
448 https://www.researchgate.net/publication/303460064_The_cyclic_and_fracture_response_of_sea_ice_in_McMurdo

449   _Sound_Part_II (Accessed 14 January 2020), 2003.

450   Elvin, A. A. and Shyam Sunder, S.: Microcracking due to grain boundary sliding in polycrystalline ice under

451   uniaxial compression, Acta Mater., 44(1), 43–56, doi:10.1016/1359-6454(95)00157-1, 1996.

452   Evans, R. J. and Untersteiner, N.: Thermal cracks in floating ice sheets, J. Geophys. Res., 76(3), 694–703,

453   doi:10.1029/JC076i003p00694, 1971.

454   Frankenstein, G. and Garner, R.: Equations for Determining the Brine Volume of Sea Ice from −0.5° to −22.9°C., J.

455   Glaciol., 6(48), 943–944, doi:10.3189/S0022143000020244, 1967.

456   Golding, N., Snyder, S. A., Schulson, E. M. and Renshaw, C. E.: Plastic faulting in saltwater ice, J. Glaciol.,

457   60(221), 447–452, doi:10.3189/2014JoG13J178, 2014.

458   Goldsby, D. L. and Kohlstedt, D. L.: Grain boundary sliding in fine-grained ice I, Scr. Mater., 37(9), 1399–1406,

459   doi:10.1016/S1359-6462(97)00246-7, 1997.

460   Gupta, V., Bergström, J. and Picu, C. R.: Effect of step-loading history and related grain-boundary fatigue in

461   freshwater columnar ice in the brittle deformation regime, Philos. Mag. Lett., 77(5), 241–247,

462   doi:10.1080/095008398178372, 1998.

463   Haskell, T. G., Robinson, W. H. and Langhorne, P. J.: Preliminary results from fatigue tests on in situ sea ice beams,

464   Cold Reg. Sci. Technol., 24(2), 167–176, doi:10.1016/0165-232X(95)00015-4, 1996.

465   Hendrikse, H. and Metrikine, A.: Edge indentation of ice with a displacement-controlled oscillating cylindrical

466   structure, Cold Reg. Sci. Technol., 121, 100–107, doi:10.1016/j.coldregions.2015.10.013, 2016.

467   Hwang, B., Wilkinson, J., Maksym, E., Graber, H. C., Schweiger, A., Horvat, C., Perovich, D. K., Arntsen, A. E.,

468   Stanton, T. P., Ren, J. and Wadhams, P.: Winter-to-summer transition of Arctic sea ice breakup and floe size

469   distribution in the Beaufort Sea, Elem Sci Anth, 5, 40, doi:10.1525/elementa.232, 2017.

470   Iliescu, D. and Schulson, E. M.: Brittle compressive failure of ice: Monotonic versus cyclic loading, Acta Mater.,

471   50(8), 2163–2172, doi:10.1016/S1359-6454(02)00060-5, 2002.

472   Iliescu, D., Murdza, A., Schulson, E. M. and Renshaw, C. E.: Strengthening ice through cyclic loading, J. Glaciol.,

473   63(240), 663–669, doi:10.1017/jog.2017.32, 2017.

474   Jordaan, I. J.: Mechanics of ice–structure interaction, Eng. Fract. Mech., 68(17–18), 1923–1960, doi:10.1016/S0013-

475   7944(01)00032-7, 2001.

476   Jordaan, I. J., Xiao, J., Wells, J. and Derradji-Aouat, A.: Ice crushing and cyclic loading in compression, in 19th

477   IAHR International Symposium on Ice, pp. 1097–1106., 2008.

478   Karulina, M., Karulin, E. and Marchenko, A.: Field investigations of first year ice mechanical properties in North-

479   West Barents Sea, in Proceedings of the 22nd International Conference on Port and Ocean Engineering under Arctic

480   Conditions, pp. 1–11, Espoo., 2013.

481   Karulina, M., Marchenko, A., Karulin, E., Sodhi, D., Sakharov, A. and Chistyakov, P.: Full-scale flexural strength

482   of sea ice and freshwater ice in Spitsbergen Fjords and North-West Barents Sea, Appl. Ocean Res., 90,

483   doi:10.1016/j.apor.2019.101853, 2019.

484   Kohout, A. L., Williams, M. J. M., Toyota, T., Lieser, J. and Hutchings, J.: In situ observations of wave-induced sea

485   ice breakup, Deep. Res. Part II Top. Stud. Oceanogr., 131, 22–27, doi:10.1016/j.dsr2.2015.06.010, 2016.

486   Langhorne, P. J. and Haskell, T. G.: Acoustic emission during fatigue experiments on first year sea ice, Cold Reg.
487   Sci. Technol., 24(3), 237–250, doi:10.1016/0165-232X(95)00021-3, 1996.

488   Langhorne, P. J., Squire, V. A., Fox, C. and Haskell, T. G.: Break-up of sea ice by ocean waves, Ann. Glaciol., 27,
489   438–442, doi:10.3189/S0260305500017869, 1998.

490   Langhorne, P. J., Squire, V. A. and Haskell, T. G.: Role of fatigue in wave-induced break-up of sea ice- a review, in
491   Ice in Surface Waters: Proceedings of the 14th International Symposium on Ice, pp. 1019–1023, Rotterdam, The
492   Netherlands., 1999.

493   Langhorne, P. J., Squire, V. A., Fox, C. and Haskell, T. G.: Lifetime estimation for a land-fast ice sheet subjected to
494   ocean swell, Ann. Glaciol., 33, 333–338, doi:10.3189/172756401781818419, 2001.

495   Lishman, B., Marchenko, A., Sammonds, P. and Murdza, A.: Acoustic emissions from in situ compression and
496   indentation experiments on sea ice, Cold Reg. Sci. Technol., 172, 102987, doi:10.1016/j.coldregions.2019.102987,
497   2020.

498   Liu, A. K., Mollo-Christensen, E., Liu, A. K. and Mollo-Christensen, E.: Wave Propagation in a Solid Ice Pack, J.
499   Phys. Oceanogr., 18, 1702–1712, doi:10.1175/1520-0485(1988)018<1702:WPIASI>2.0.CO;2, 1988.

500   Masterson, D.: The Story of Offshore Arctic Engineering - Dan Masterson - Google Books, Cambridge Scholars
501   Publishing.   [online]   Available   from:
502   https://books.google.com/books/about/The_Story_of_Offshore_Arctic_Engineering.html?id=y9N1DwAAQBAJ
503   (Accessed 4 March 2021), 2018.

504   Michel, B. and Ramseier, R. O.: Classification of river and lake ice, Can. Geotech. J., 8(1), 36–45, doi:10.1139/t71-
505   004, 1971.

506   Mulmule, S. V. and Dempsey, J. P.: Stress-Separation Curves for Saline Ice Using Fictitious Crack Model, J. Eng.
507   Mech., 123(8), 870–877, doi:10.1061/(asce)0733-9399(1997)123:8(870), 1997.

508   Murdza, A., Marchenko, A., Sakharov, A., Chistyakov, P., Karulin, E. and Karulina, M.: Test with L-shaped
509   cantilever beam for complex shear and bending strength, in 23rd IAHR International Symposium on Ice, pp. 1–9,
510   Ann Arbor, Michigan, USA., 2016.

511   Murdza, A., Schulson, E. M. and Renshaw, C. E.: Hysteretic behavior of freshwater ice under cyclic loading:
512   preliminary results, in 24th IAHR International Symposium on Ice, pp. 185–192, Vladivostok., 2018.

513   Murdza, A., Schulson, E. M. and Renshaw, C. E.: The effect of cyclic loading on the flexural strength of columnar
514   freshwater ice, in Proceedings of the International Conference on Port and Ocean Engineering under Arctic
515   Conditions, POAC, vol. 2019-June., 2019.

516   Murdza, A., Marchenko, A., Schulson, E., Renshaw, C., Sakharov, A., Karulin, E. and Chistyakov, P.: Results of
517   preliminary cyclic loading experiments on natural lake ice and sea ice, in 25th IAHR International Symposium on
518   Ice, pp. 1–10, Trondheim, Norway., 2020a.

519   Murdza, A., Schulson, E. M. and Renshaw, C. E.: Strengthening of columnar-grained freshwater ice through cyclic
520   flexural loading, J. Glaciol., 66(258), 556–566, doi:10.1017/jog.2020.31, 2020b.

521   Murdza, A., Marchenko, A., Schulson, E. M. and Renshaw, C. E.: Cyclic strengthening of lake ice, J. Glaciol.,
522   67(261), 182–185, doi:10.1017/jog.2020.86, 2021.

523   O'Rourke, B. J., Jordaan, I. J., Taylor, R. S. and Gürtner, A.: Experimental investigation of oscillation of loads in ice

524   high-pressure zones, part 1: Single indentor system, Cold Reg. Sci. Technol., 124, 25–39,

525   doi:10.1016/J.COLDREGIONS.2015.12.005, 2016.

526   Pistone, K., Eisenman, I. and Ramanathan, V.: Observational determination of albedo decrease caused by vanishing

527   Arctic sea ice, Proc. Natl. Acad. Sci. U. S. A., 111(9), 3322–3326, doi:10.1073/pnas.1318201111, 2014.

528   Prinsenberg, S. J. and Peterson, I. K.: Observing regional-scale pack-ice decay processes with helicopter-borne

529   sensors and moored upward-looking sonars, Ann. Glaciol., 52(57), 35–42, doi:10.3189/172756411795931688,

530   2011.

531   Richter-Menge, J. A. and Jones, K. F.: The tensile strength of first-year sea ice, J. Glaciol., 39(133), 609–618,

532   doi:10.3189/S0022143000016506, 1993.

533   Sammis, C. G. and Ashby, M. F.: The failure of brittle porous solids under compressive stress states, Acta Metall.,

534   34(3), 511–526, doi:10.1016/0001-6160(86)90087-8, 1986.

535   Schijve, J.: Fatigue of Structures and Materials, 2nd ed., Springer Netherlands., 2009.

536   Schulson, E. M. and Duval, P.: Creep and Fracture of Ice, Cambridge University Press, Cambridge., 2009.

537   Schulson, E. M., Kuehn, G. A., Jones, D. A. and Fifolt, D. A.: The growth of wing cracks and the brittle

538   compressive failure of ice, Acta Metall. Mater., 39(11), 2651–2655, doi:10.1016/0956-7151(91)90081-B, 1991.

539   Schulson, E. M., Qi, S., Melton, J. S. and Gratz, E. T.: Across-column cracks and axial splits in S2 saline ice under

540   compression, J. Glaciol., 43(145), 411–414, doi:10.3189/s0022143000034997, 1997.

541   Shackleton, E. H.: South: The Story of Shackleton's Last Expedition, 1914–17, Macmillian, USA., 1982.

542   Squire, V. A.: Of ocean waves and sea-ice revisited, Cold Reg. Sci. Technol., 49(2), 110–133,

543   doi:10.1016/j.coldregions.2007.04.007, 2007.

544   Suresh, S.: Fatigue of Materials, Cambridge University Press., 1998.

545   Tabata, T. and Nohguchi, Y.: Failure of Sea Ice by Repeated Compression, in Physics and Mechanics of Ice, pp.

546   351–362, Springer Berlin Heidelberg, Berlin, Heidelberg., 1980.

547   Timco, G. W. and O'Brien, S.: Flexural strength equation for sea ice, Cold Reg. Sci. Technol., 22(3), 285–298,

548   doi:10.1016/0165-232X(94)90006-X, 1994.

549   Weeks, W. F.: On Sea Ice, University of Alaska Press., 2010.

550   Weeks, W. F. and Ackley, S. F.: The Growth, Structure, and Properties of Sea Ice, in The Geophysics of Sea Ice, pp.

551   9–164, Springer US, Boston, MA., 1986.

552   Wei, M., Polojärvi, A., Cole, D. M. and Prasanna, M.: Strain response and energy dissipation of floating saline ice

553   under cyclic compressive stress, Cryosph., 14(9), 2849–2867, doi:10.5194/tc-14-2849-2020, 2020.

554   Weiss, J. and Schulson, E. M.: Grain-boundary sliding and crack nucleation in ice, Philos. Mag. A, 80(2), 279–300,

555   doi:10.1080/01418610008212053, 2000.

556   Zhang, R., Wang, H., Fu, Q., Rasch, P. J. and Wang, X.: Unraveling driving forces explaining significant reduction

557   in satellite-inferred Arctic surface albedo since the 1980s, Proc. Natl. Acad. Sci. U. S. A., 116(48), 23947–23953,

558   doi:10.1073/pnas.1915258116, 2019.

559

560
561
562
563
564
565
566
567
568
569
570
571

Table 1. Physical properties of as-grown saline ice.

Material	Density [kg m^{-3}]	Average salinity [ppt]	Grain size [mm]
Saline ice (lower salinity)	878±11	3.0±0.9	3.8±0.9
Saline ice (higher salinity)	897±10	5.9±0.6	3.6±1.1

573
574
575
576

Table 2. Flexural strength of non-cycled saline ice at -10°C and a displacement rate of 0.1 mm/s.

Flex strength of ice of lower salinity (3.0±0.9 ppt) [MPa]	Depth [cm]	Flex strength of ice of higher salinity (5.9±0.6 ppt) [MPa]	Depth [cm]
1.08	—	0.45	20 – 22.5
0.86	—	0.53	17.5 – 20
1.06	—	0.62	12.5 – 15
0.96	—	0.98	7.5 – 10
0.83	17 – 21	1.17	5 – 7.5
0.75	13.5 – 17	1.26	5 – 7.5
1.08	10 – 13.5	1.26	2.5 – 5
0.97	6.5 – 10	1.44	1 – 2.5
1.09	3 – 6.5	1.17	—
Average		Average	
0.96±0.13		0.98±0.36	

578
579
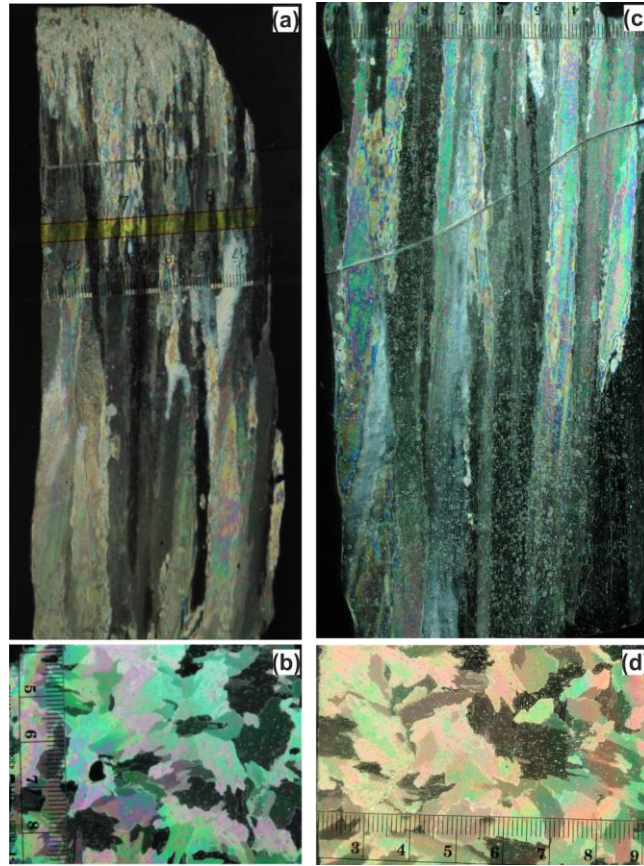
580
581 **Figure 1. Photographs of a vertically-oriented (a) and a horizontally-oriented (b) thin-sections (~1mm) of columnar-**
582 **grained, saline ice of lower salinity (3.0±0.9 ppt) as viewed between crossed-polarized filters; photographs of a vertically-**
583 **oriented (c) and a horizontally-oriented (d) thin-sections of saline ice of higher salinity (5.9±0.6 ppt).**
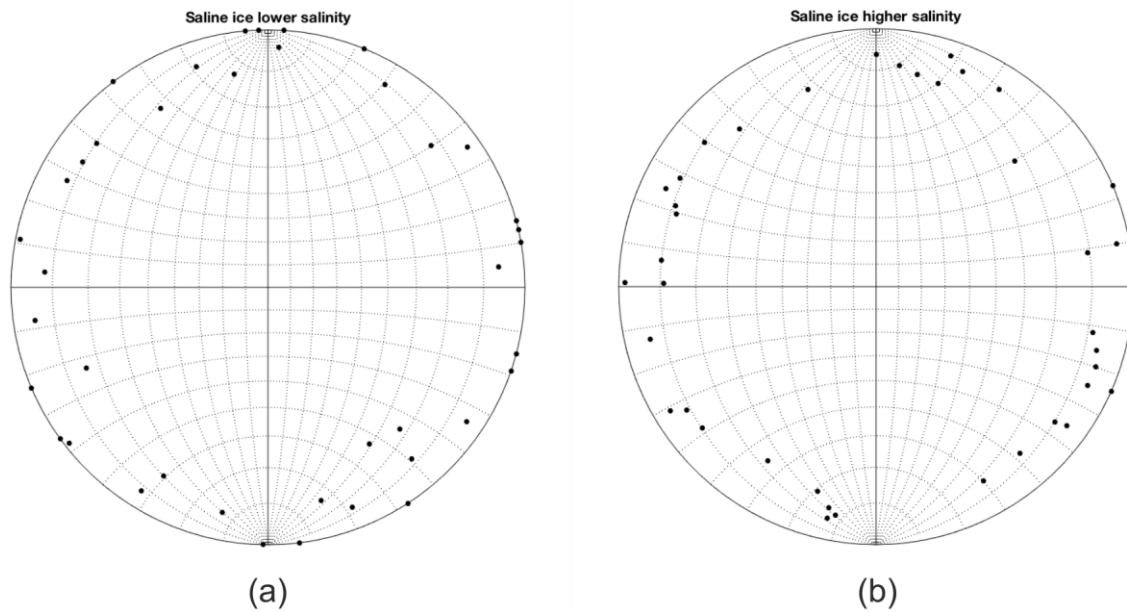
584
585 **Figure 2. Stereographic projection plots of crystal c-axis {0001} orientations in saline ice of lower (3.0±0.9 ppt) salinity (a)**
586 **and saline ice of higher (5.9±0.6 ppt) salinity (b).**
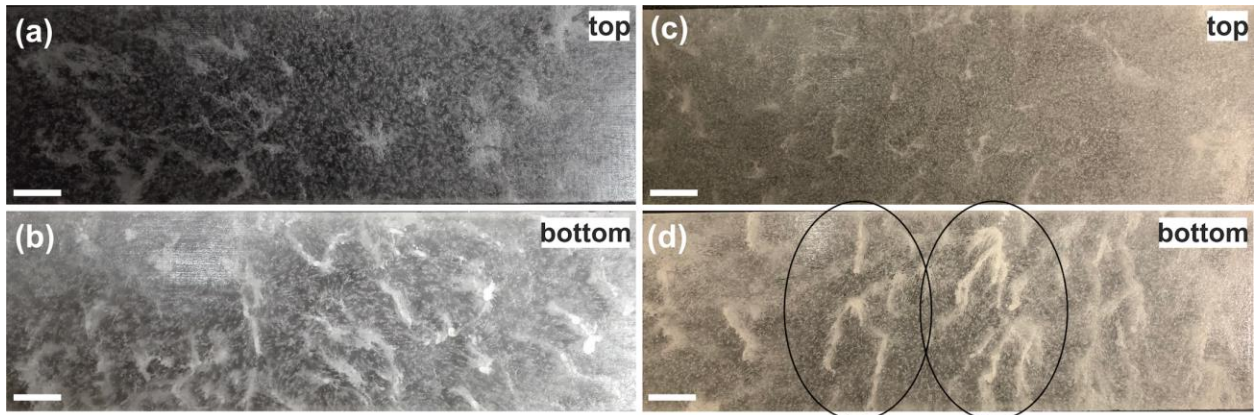
587
588 **Figure 3. Photographs of saline ice samples of lower salinity (3.0±0.9 ppt) from the top (a) and bottom (b) of an ice block**
589 **and saline ice samples of higher salinity (5.9±0.6 ppt) from the top (c) and bottom (d) of an ice block. The concentration of**
590 **whitish features along the width of a sample in (d) is shown inside circles which is a predominant place for a crack to**
591 **initiate. The columnar grains run in and out of the images. Scale bars: 20 mm.**
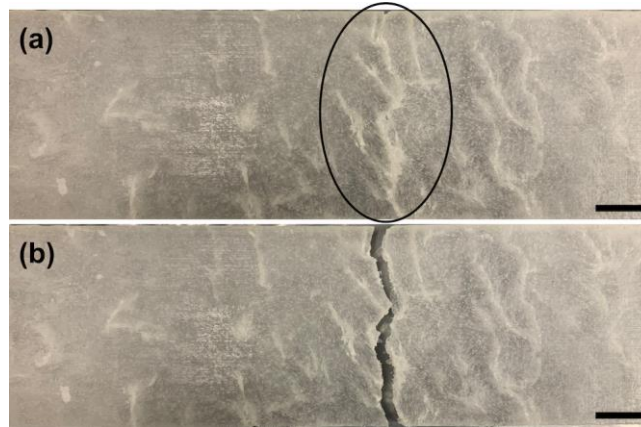
592
593 **Figure 4. Photograph of a sample from the bottom of an ice block of higher salinity (5.9±0.6 ppt) before cycling (a) and**
594 **after (b) failure. Note a crack that propagated along whitish features in the area in (a) depicted by the circle. Scale bars:**
595 **20 mm.**

(a)   (b)
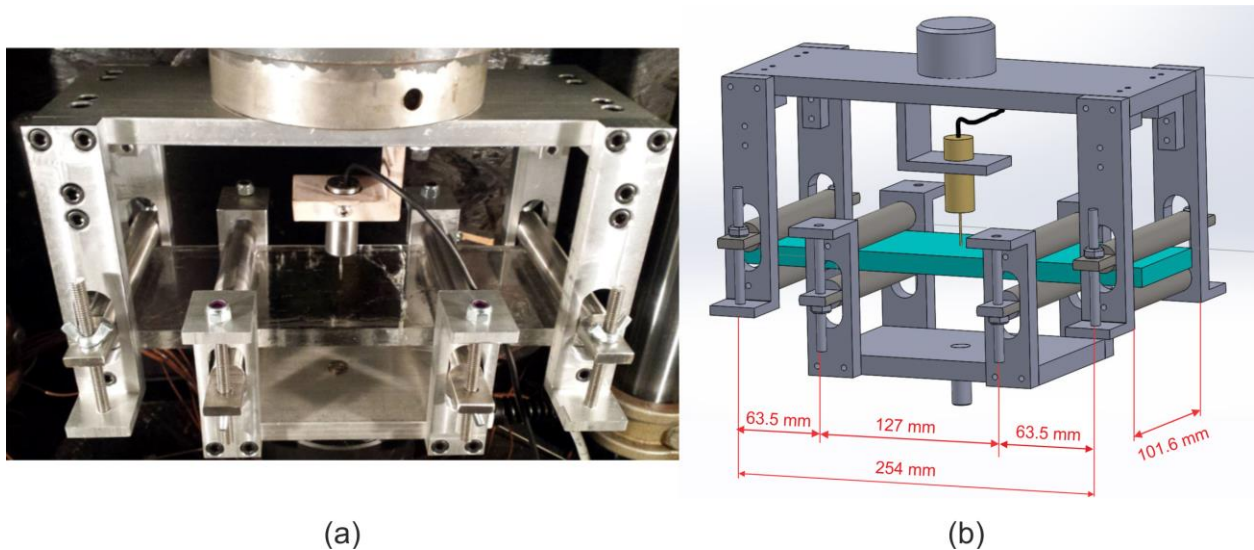
596
597 **Figure 5. Photograph (a) and sketch (b) of the four-point bending apparatus connected to an MTS hydraulic testing**
598 **system** (Iliescu et al., 2017; Murdza et al., 2020b)**. The upper part is attached to the frame of the machine while the mobile**

599   **middle part is attached through a fatigue-rated load cell to the piston. The apparatus is made from an aluminum alloy;**
600   **the loading cylinders are made from stainless steel.**
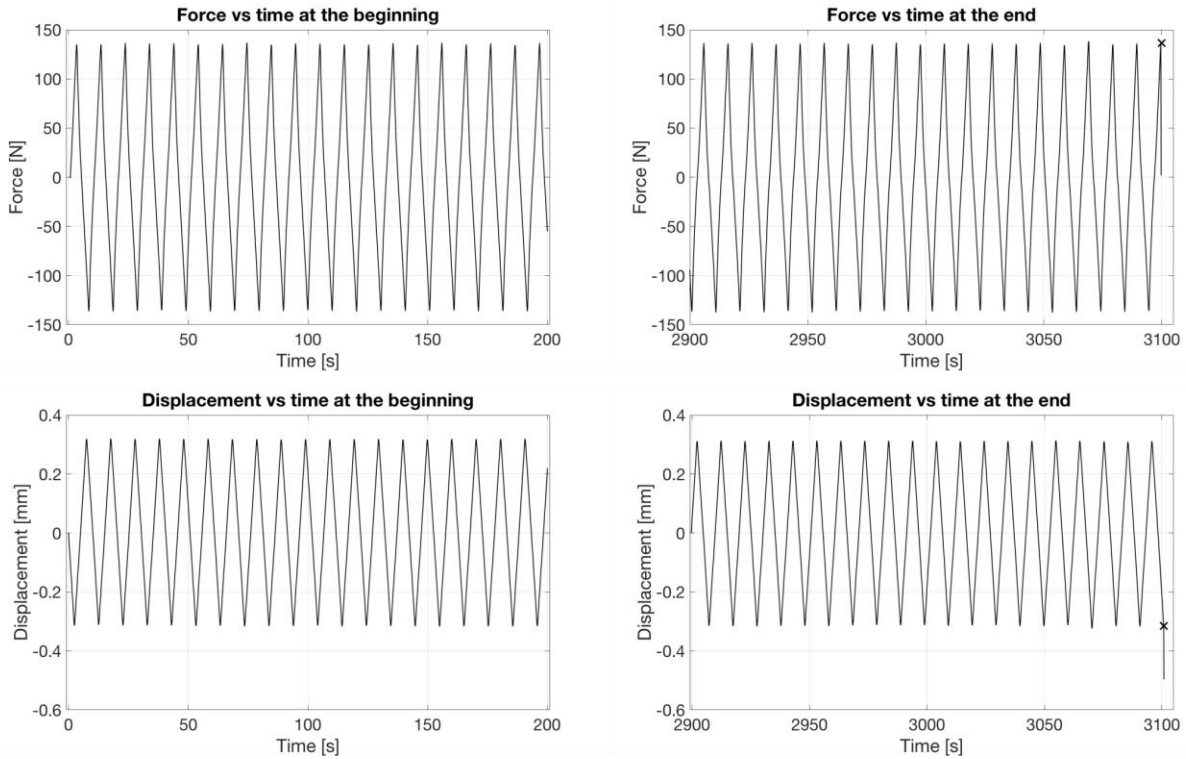
601
602   **Figure 6. Curves of force/load and displacement vs. time for periods of 200 s near the beginning and near the end of**
603   **cycling before fatigue failure occurred. Marker symbol "x" denotes a moment of specimen failure. Force of ~135 N**
604   **corresponds to ~1.2 MPa.**
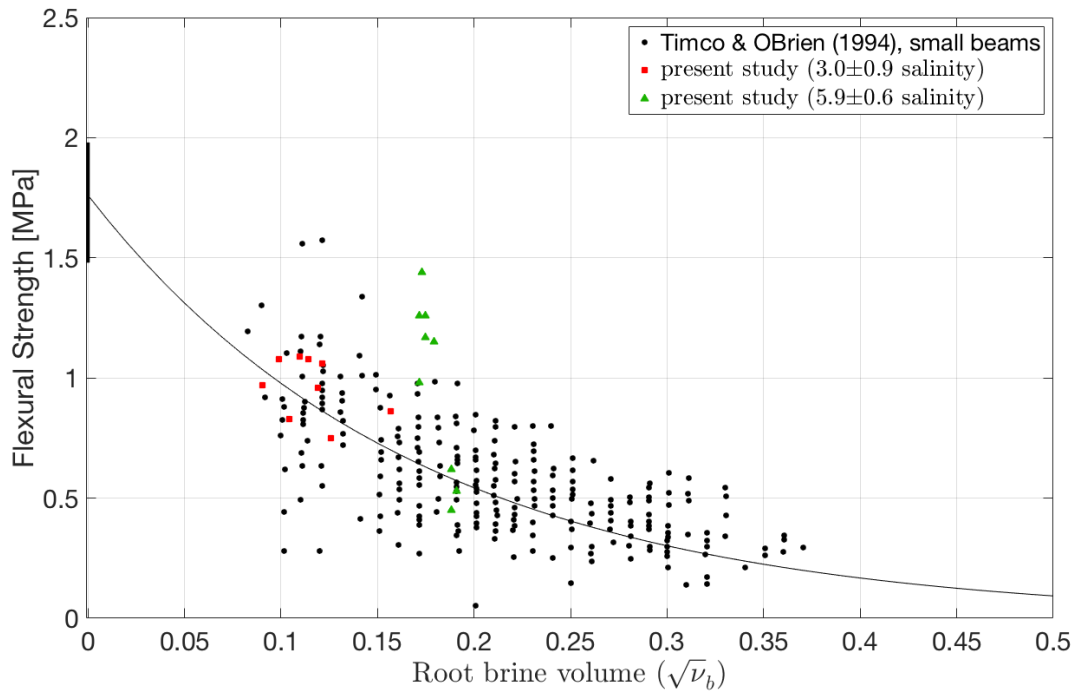
605
606 **Figure 7. Flexural strength of saline ice as a function of root brine volume for the ice grown in the present study and for**
607 **data from Timco and O'Brien (1994) for comparison.**
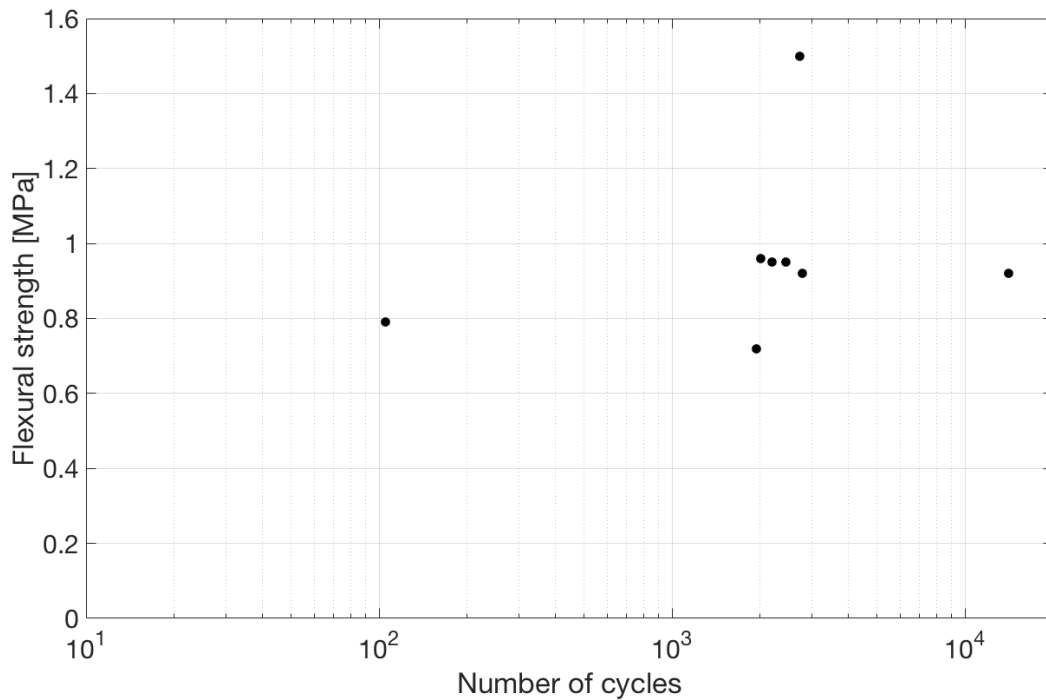
608
609 **Figure 8. Flexural strength and the corresponding number of cycles imposed for saline ice of lower salinity (3.0±0.9) ppt**
610 **cycled at 0.35 MPa outer-fiber stress amplitude at -10 ºC and 0.1 mm s⁻¹ outer-fiber center-point displacement rate.**
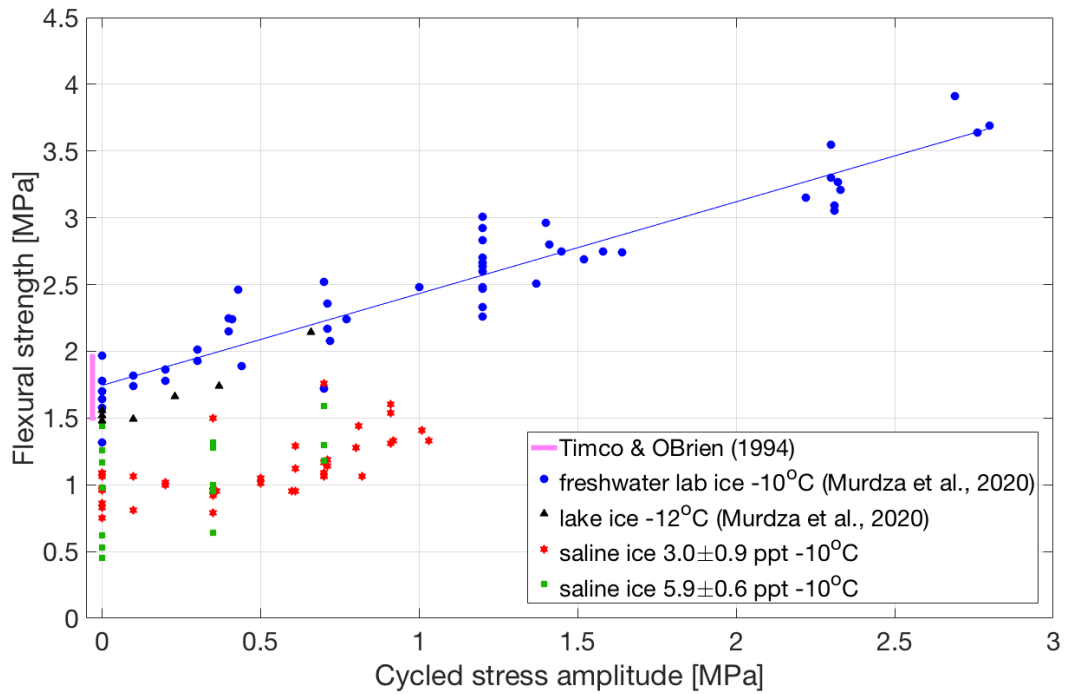
611
Figure 9. Flexural strength of freshwater ice and saline ice of lower (3.0±0.9 ppt) and of higher (5.9±0.6 ppt) salinity as a function of reverse-cycled stress amplitude. Freshwater ice laboratory and lake data are taken from (Murdza et al., 2020b, 2021). Red five-pointed stars and green squares represent tests performed on saline ice of lower and higher salinities, respectively, at 0.1 mm s⁻¹ and -10°C. During all depicted tests the ice did not fail during cycling and was broken by applying one unidirectional displacement until failure occurred.
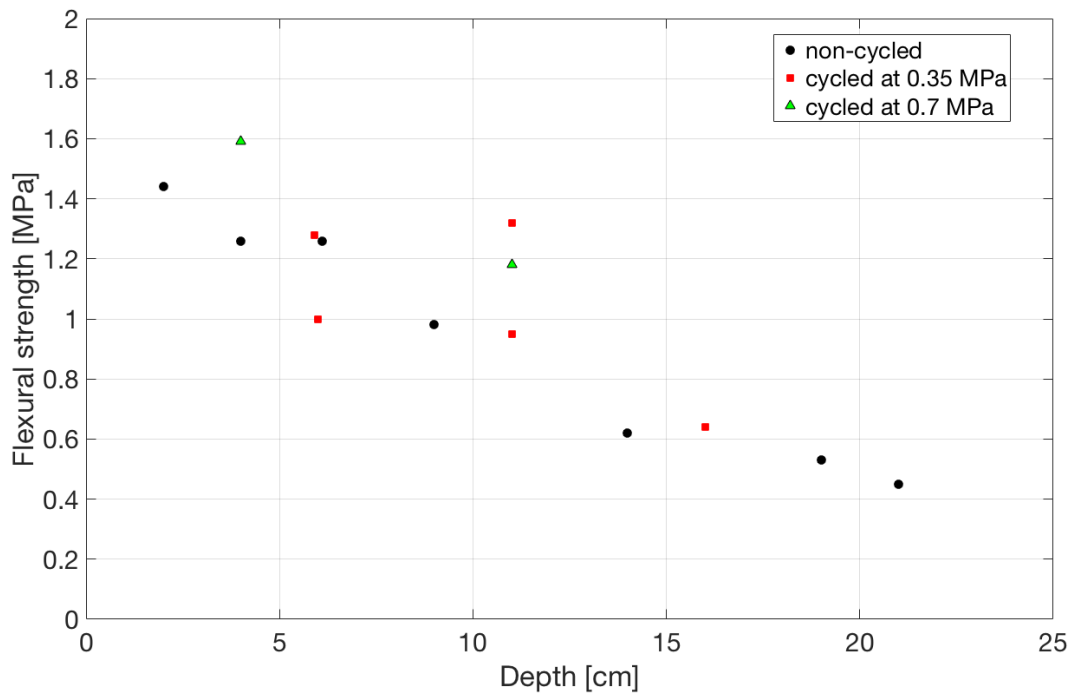
617
Figure 10. Flexural strength as a function of position of saline ice samples of higher salinity (5.9±0.6 ppt) for different cyclic amplitudes. The imposed number of cycles for specimens cycled at 0.35 and 0.7 MPa is ~2000.
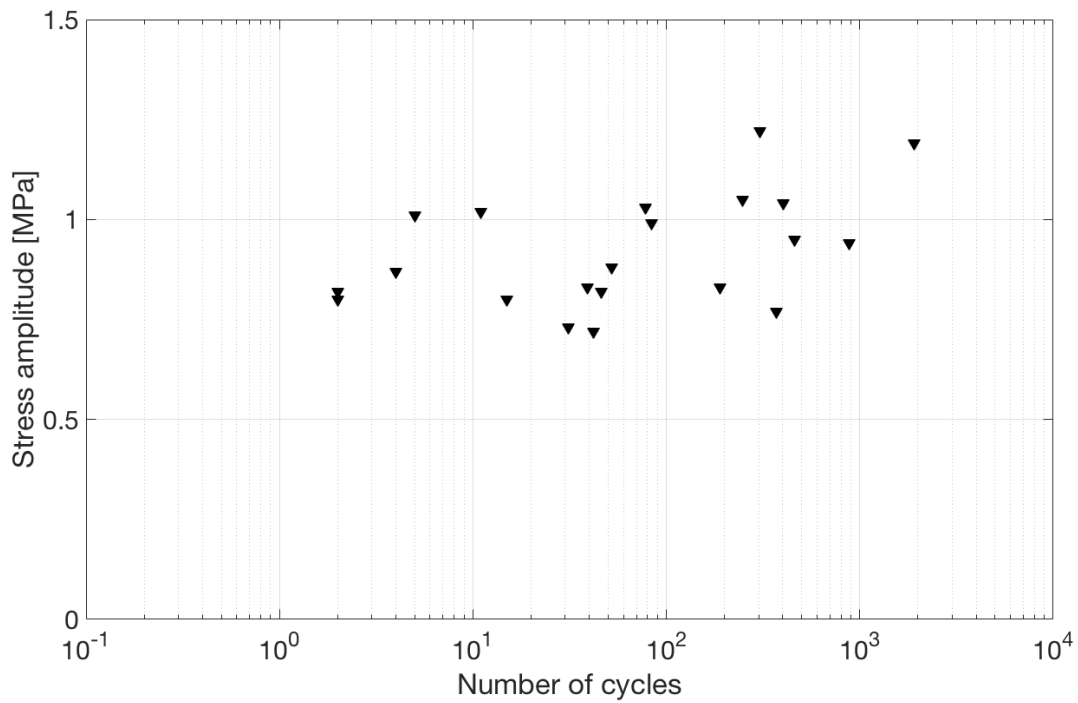
620
621 **Figure 11. Stress amplitude as a function of the number of cycles to fatigue fracture for saline ice of lower salinity**
622 **(3.0±0.9 ppt) tested at -10ºC and 0.1 mm s⁻¹ outer-fiber center-point displacement rate.**

623
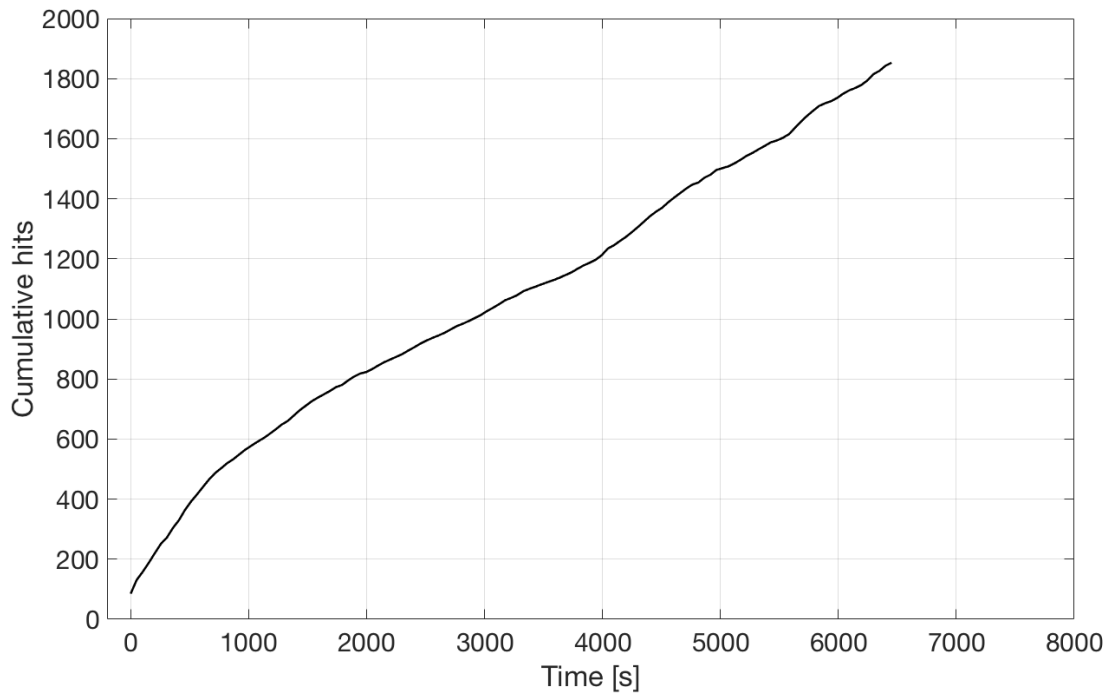
624
625 **Figure 12. Acoustic emissions (hits) against time for saline ice of lower salinity (3.0±0.9 ppt), cycled at a stress amplitude**
626 **of 0.5 MPa at -10ºC at an outer-fiber displacement rate of 0.1 mm s⁻¹.**
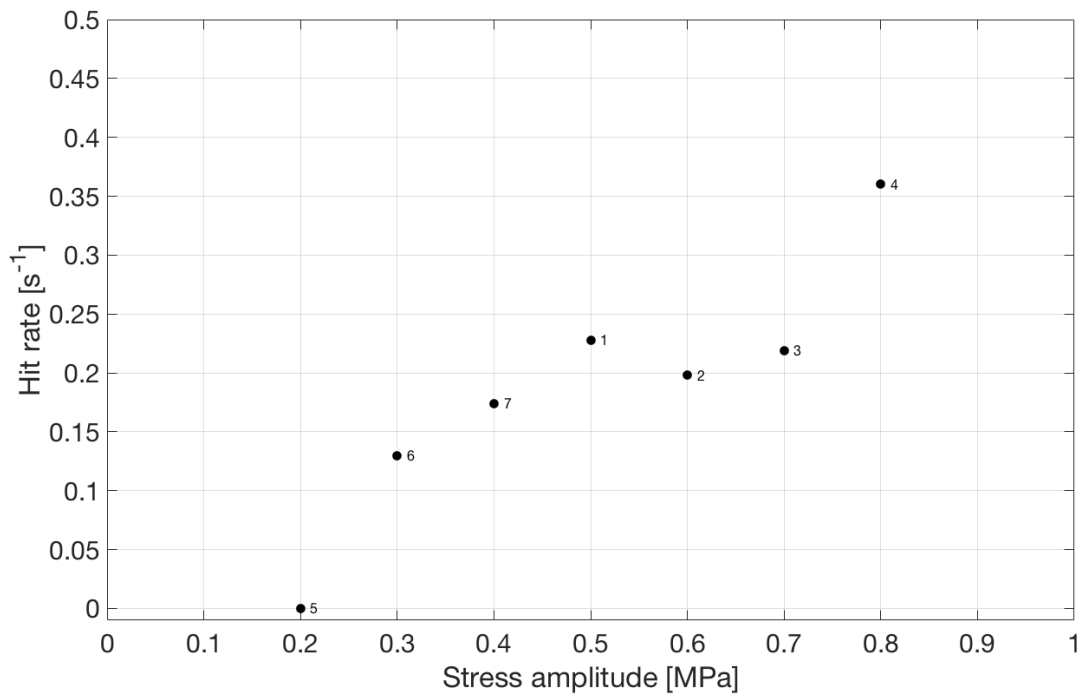
627
628 **Figure 13. Hit rate as a function of cycled stress amplitude for saline ice sample of lower salinity (3.0±0.9 ppt). Numbers**
629 **show the order of cycling at different stress amplitudes.**

630
631
632